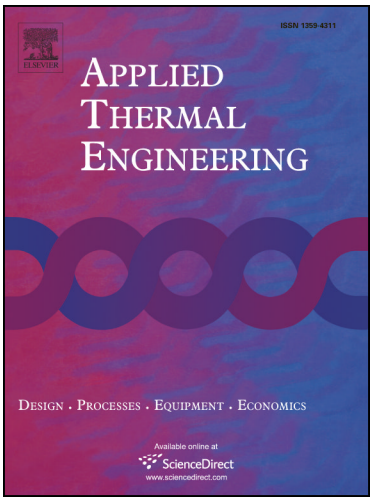

Thermal Behaviour of Medium-voltage Underground Cables under High-load Operating Conditions

S. Bustamante, R. Mínguez, A. Arroyo, M. Manana, A. Laso, P. Castro, R. Martínez

PII: S1359-4311(18)36375-0
DOI: https://doi.org/10.1016/j.applthermaleng.2019.04.083
Reference: ATE 13673

To appear in: *Applied Thermal Engineering*

Received Date: 18 October 2018
Accepted Date: 19 April 2019

Please cite this article as: S. Bustamante, R. Mínguez, A. Arroyo, M. Manana, A. Laso, P. Castro, R. Martínez, Thermal Behaviour of Medium-voltage Underground Cables under High-load Operating Conditions, *Applied Thermal Engineering* (2019), doi: https://doi.org/10.1016/j.applthermaleng.2019.04.083

Thermal Behaviour of Medium-voltage Underground Cables under High-load Operating Conditions

S. Bustamante[1], R. Mínguez[◊], A. Arroyo, M. Manana, A. Laso, P. Castro, R. Martínez

University of Cantabria, Department of Electrical and Energy Engineering, Av. Los Castros s/n., 39005 Santander, Spain

◊ Viesgo Distribución Eléctrica S.L., Calle Isabel Torres 25, 39011 Santander, Spain

Abstract

The dynamic management of electric power distribution lines has become a topic of great interest at present. Knowledge of the ampacity of cables is fundamental to carrying out dynamic management. In this study, the ampacity of buried cables in different soil resistivities and depths was calculated. A small-scale model was built in the laboratory to simulate the operating conditions of a buried cable. With the experimental results, a numerical model based on the finite element method was validated to evaluate the ampacities calculated by two standards. A comparison was made between the ampacities calculated from the IEC 60287-1 and UNE 211435 standards and those obtained from the simulated model. In addition, a comparison was made regarding the steady-state temperatures obtained at each calculated ampacity. The results obtained from the simulated model design show that the ampacity calculation method of the IEC 60287-1 standard where drying-out of the soil occurs is the most accurate, and has the least risk of exceeding the maximum permissible cable temperature.

Keywords: ampacity, underground cable, finite element method model, thermal analysis

1. Introduction

Energy consumption and the need for necessary infrastructure to distribute electrical energy where demanded is growing. This is where the dynamic management of electric power distribution lines comes into play because it allows operation above the static capacity of a conductor. According to CIGRE TB 338 [**?**], the costs of installing underground cable tends to be significantly higher in urban areas than in rural areas, so this management model can offer more capacity when needed without installing additional lines. In addition, it offers support to networks against line breakdowns and maintenance tasks because it allows

[1]Corresponding author.
E-mail address: sergio.bustamante@unican.es (S. Bustamante)

energy to be derived through alternative lines without overloading them above their maximum permissible temperature.

Underground cable lines with cross-linked polyethylene insulation are currently widely used for the supply of energy to cities and industries in many countries. In addition to new installations, they are also used to replace old overhead power lines in cities. The first step in exploiting power supply lines dynamically is to know a cable's ampacity. The cable ampacity is the maximum allowable current that can circulate through a conductor without damaging the insulation of the cable [**?**]. Thus, temperature control of the cable insulation prevents rapid aging and emergency situations. Knowing the cable ampacity, the load curve and the ambient temperature of the soil makes it possible to apply the equations of IEC 60853-1 [**?**] to calculate the cyclic transport factor to exploit a line dynamically without exceeding the maximum admissible temperature of the cable. It also provides an orientation of the value of current that can circulate through a cable in case of emergency using the equations of IEC 60853-2 [**?**]. An example of this calculation can be seen in [**? ?**], where the study of the cyclic load factor in a medium-voltage power cable in flat formation was made.

Several studies [**? ?**] have addressed the issue of cable ampacity calculation and the obtainment of the thermal properties of cables using the concept of thermal impedance in buried copper cables or in conduits. Some studies [**? ?**] use standards of their countries derived from IEC 60287 or simplified formulas to perform the theoretical study of the ampacity of medium-voltage underground cables. Other studies [**? ? ? ? ? ? ? ? ? ? ? ?**] have used the finite element method (FEM) to calculate cable ampacity and thermal behaviour of a cable using single- or multi-core cables buried or in ducts and in trefoil or flat formation and have observed the effect of the variation of soil resistivity.

In this study, a small-scale model of a buried aluminium cable was constructed to validate the results obtained by the FEM. After validation of the FEM, a comparison was made between the cable ampacity results obtained from IEC 60287, UNE 211435 and through the FEM. Finally, a study of the generated magnetic field was performed based on the ampacity values and installation depths.

2. Theoretical model

In Spain, the value of the permissible current rating of a buried cable can be obtained from several international and national standards. In this study, the methods described in IEC 60287-1-1 [**?**] and UNE 211435 [**?**] for the ampacity calculation of underground cables were followed.

According to IEC 60287-1-1 [**?**], to calculate the permissible current rating, it is necessary to perform the calculation in conditions of partial drying-out of the soil and in conditions where drying-out of the soil does not occur, and the lowest of the two currents obtained is used.

The permissible AC current rating of a buried cable where drying-out of the soil does not occur is given

as

$$I = \left[\frac{\Delta\theta - W_d[0.5T_1 + n(T_2 + T_3 + T_4)]}{RT_1 + nR(1+\lambda_1)T_2 + nR(1+\lambda_1+\lambda_2)(T_3+T_4)}\right]^{0.5} \quad (1)$$

where, I is the current flowing in one conductor (A), $\Delta\theta$ is the conductor temperature rise above the ambient temperature (K); R is the AC resistance per unit length of the conductor at maximum operating temperature (Ω/m); W_d is the dielectric loss per unit length for the insulation surrounding the conductor (W/m), T_1, T_2, T_3 and T_4 are the thermal resistances per unit length between one conductor and the sheath, the bedding between the sheath and armour, the external serving of the cable and between the cable surface and the surrounding medium $(K \cdot m/W)$, respectively; n is the number of load-carrying conductors in the cable (conductors of equal size carrying the same load); λ_1 is the ratio of losses in the metal sheath to total losses in all conductors in that cable and λ_2 is the ratio of losses in the armouring to total losses in all conductors in that cable.

The permissible AC current rating of a buried cable where partial drying-out of the soil occurs is given as

$$I = \left[\frac{\Delta\theta - W_d[0.5T_1 + n(T_2 + T_3 + vT_4)] + (v-1)\Delta\theta_x}{R[T_1 + n(1+\lambda_1)T_2 + n(1+\lambda_1+\lambda_2)(T_3+vT_4)]}\right]^{0.5} \quad (2)$$

where, v is the ratio of the thermal resistivities of the dry and moist soil zones ($v = \rho_d/\rho_w$), ρ_d is the thermal resistivity of dry soil $(K \cdot m/W)$, ρ_w is the thermal resistivity of moist soil $(K \cdot m/W)$, $\Delta\theta_x$ is the temperature rise of the boundary between the dry and moist zones above the ambient temperature of the soil $(\theta_x - \theta_a)$ (K), θ_x is the critical temperature of soil and temperature of the boundary between the dry and moist zones $(^\circ C)$ and θ_a is the ambient temperature $(^\circ C)$.

The AC resistance of a conductor at maximum operating temperature (Ω/m) is calculated as

$$R = R_0[1 + \alpha_{20}(\theta - 20)](1 + y_s + y_p) \quad (3)$$

where, R_0 is the DC resistance of the conductor at 20 $^\circ C$ (Ω/m), α_{20} is the constant mass temperature coefficient at 20 $^\circ C$ per kelvin, θ is the cable maximum operating temperature $(^\circ C)$ and y_s and y_p are the skin and proximity effect factors, respectively, that can be calculated using the expressions given in [**?**].

The expressions to calculate the thermal resistances per unit length were obtained from IEC 60287-2-1 [**?**], the thermal resistance of the bedding between the sheath and armour was zero because the cable did not have armour (as described in Section 3, Material and method). T_1, T_3 and T_4 were calculated as

$$T_1 = \frac{\rho_T}{2\pi} ln\left[1 + \frac{2t_1}{d_c}\right] \quad (4)$$

$$T_3 = \frac{1}{2\pi}\rho_T ln\left(1 + \frac{2t_3}{D'_a}\right) \quad (5)$$

$$T_4 = \frac{1}{2\pi}\rho_T[ln(2u) + 2ln(u)] \quad (6)$$

where, ρ_T is the thermal resistivity of material (thermal resistivity of insulation for T_1 and T_3, and thermal resistivity of sand for T_4) $(K \cdot m/W)$, d_c is the diameter of the conductor (mm), t_1 is the thickness of insulation between the conductor and sheath (mm), t_3 is the thickness of serving (mm), D'_a is the external diameter of the component immediately beneath the outer covering (mm), $u = \frac{2L}{D_e}$, L is the distance from the surface of the ground to the centre of the trefoil group (mm) and D_e is the external diameter of one cable (mm).

The ratio of losses in the metal sheath to the total losses in all conductors in the cable is given by

$$\lambda_1 = \lambda'_1 + \lambda''_1 \ , \qquad \lambda'_1 = \frac{R_s}{R} \frac{1}{1 + \left(\frac{R_s}{X}\right)^2} \tag{7}$$

where, λ'_1 are the losses caused by circulating currents, λ''_1 are the losses caused by eddy currents ($\lambda''_1 = 0$, eddy current loss is ignored according to [**?**]), R_s is the resistance of the sheath per unit length of cable at its maximum operating temperature (Ω/m), X is the reactance per unit length of sheath per unit length of cable (Ω/m) $X = 2\omega 10^{-7} ln(\frac{2s}{d})$, s is the distance between the conductor axes (mm) and d is the mean diameter of the sheath (mm).

As in the case of the thermal resistance of the bedding between the sheath and armour (T_2), the ratio of losses in the armour to the total losses in all conductors in the cable (λ_2) was zero because there was no armour in the cable.

The power losses generated inside the cable occur in the conductor, in the insulation and on the sheath. The conductor loss is generated by the current flowing through the resistance of the conductor, the dielectric loss is caused by the voltage through the insulation and the sheath loss is caused by currents induced in the sheath [**?**].

The volumetric heat source per the cable conductor unit volume Q_c is calculated as

$$Q_c = \frac{I^2 R}{A_c} \tag{8}$$

where, I is the current flowing in one conductor (A), A_c is the cross-sectional area of the conductor (m^2) and R is the AC resistance per unit length of the conductor at maximum operating temperature (Ω/m).

The volumetric heat source owing to cable insulation Q_d is estimated as

$$Q_d = \frac{W_d}{A_{ins}} \ , \qquad W_d = \omega C {U_0}^2 tan\ \delta \ , \qquad A_{ins} = \pi({r_{ins}}^2 - {r_c}^2) \tag{9}$$

where, W_d is the dielectric loss per unit length for the insulation surrounding the conductor (W/m), A_{ins} is the insulation area (m^2), $\omega = 2\pi f$, C is the capacitance per unit length (F/m), U_0 is the voltage to earth (V), $tan\ \delta$ is the loss factor of the insulation at power frequency and operating temperature [**?**] and r_{ins} is the outer radius of the insulation (m).

The volumetric heat source of the sheath, Q_s, is:

$$Q_s = \frac{(\lambda_1) I^2 R}{A_{sh}} , \qquad A_{sh} = \pi({r_{sh}}^2 - {r_{ins}}^2) \tag{10}$$

where, λ_1 is the ratio of losses in the metal sheath to total losses in all conductors in the cable, A_{sh} is the sheath area (m^2) and r_{sh} is the outer radius of the sheath (m).

UNE 211435 [**?**] is a Spanish standard derived from IEC 60287-1-1 [**?**], it is used by cable manufacturers in their catalogues as guidelines and selection recommendations. UNE 211435 uses a much simpler ampacity calculation method. It starts from the maximum admissible current that depends on the type of installation and the conductor section, then several correction factors are applied. From several values of ambient temperature, soil resistivity, installation depth and number of nearby circuits, the correction factors of the maximum admissible current are obtained.

$$I = I_0 . F_{Ta} . F_{Soil} . F_{Depth} . F_{Circuit} \tag{11}$$

where, I_0 is the maximum admissible current based on the type of installation and the conductor section (A), F_{Ta} is the correction factor owing to the ambient temperature, F_{Soil} is the correction factor owing to the soil resistivity surrounding the cables, F_{Depth} is the correction factor owing to the installation depth of the cables and $F_{Circuit}$ is the correction factor owing to the number of adjacent circuits and the distance between them.

3. Material and method

In this study, the focus was on the variation of the thermal behaviour of underground cables operating in steady-state conditions at various depths.

Regarding the thermal analysis of soil around a buried power cable, a laboratory experiment simulating the operation of an underground cable was performed that obtained the temperature data around a cable for the calibration of a mathematical model, FEM in 2D.

3.1. Experimental measurements

A small-scale model was built with similar characteristics to [**? ? ? ? ?**] to simulate the operating conditions of a buried cable. The characteristics of the power distribution cable used during the experimental measurements are shown in Table 1.

The model was constructed in the form of a wooden container simulating in terms of scale the area of the ground surface covering an electrically charged cable. It was installed in an area isolated from the outside environment and air conditioning. The wooden container was 2 m long, 0.536 m wide and 0.518 m high, the thickness of the panels was 0.018 m, and the upper part was left open. The container was filled with sand

Table 1: Cable characteristics

General Cable HERSATENE RHZ1-OL 12/20kV $1x150\,mm^2$ H16 Al2	
Type of cable	AL/XLPE/CU/PE
Cross-sectional area (mm^2)	150
Conductor diameter (mm)	14
Insulation total thickness (mm)	5.5
External diameter (mm)	34
DC resistance at 20 $°C$ (Ω/km)	0.206
AC resistance at 90 $°C$ (Ω/km)	0.264
Max. conductor temperature at continuous load ($°C$)	90

and a 150 mm^2 aluminium cable with electrical insulation was installed inside at a distance of 20 cm from the sand surface. Eight temperature probes (PT100) were installed around the buried cable to obtain the temperature at different distances from the cable. The installation scheme of the cable inside the wooden container and the location of the probes around the cable are shown in Fig. 1.

Figure 1: Schematic design of buried cable and temperature probes inside sand filled container (distance expressed in mm).

To simulate the current flowing through the cable under operating conditions, two toroidal current transformers were connected in parallel and fed from a voltage source. The secondary winding of the transformers was a cable connected in a short circuit in which the currents used for power distribution were achieved.

The acquisition of data measured by the temperature probes and the intensity circulating through the cable was performed by a Raspberry Pi and several additional plates. The design and construction of this data logger was very similar to that developed in other types of research [**?**] but allowed us to obtain a fairly accurate data logger at a lower cost. Figure 2 shows the assembly and elements of the test facility.

Figure 2: Set-up for experimental analysis.

3.2. Numerical model (FEM)

To reproduce the same results observed in laboratory measurements, a mathematical model was created. The model was implemented through FEM software and was subsequently adjusted and validated based on the comparison of outputs of both software and laboratory measurements. Figure 3 shows the generated

model and the location of the temperature probes. ANSYS® [**?**] was the software used in the simulations. The heat conduction equation used to validate the model [**? ?**], was as follows:

$$\frac{\partial}{\partial x}\left(k\frac{\partial \theta}{\partial x}\right)+\frac{\partial}{\partial y}\left(k\frac{\partial \theta}{\partial y}\right)-C_v\frac{\partial \theta}{\partial t}=-q \tag{12}$$

where, θ is the temperature at any point in the x-y plane (K), k is the thermal conductivity $(W/m\cdot K)$, C_v is the specific heat per unit volume $(J/m^3\cdot K)$ and q is the volumetric heat source (W/m^3).

Figure 3: Detail of mesh around underground cable and temperature probes.

Once the model was validated, the geometry of the problem was modified using the finite element software. In this new geometry, the same thermophysical properties were maintained as in the initial model; in addition, the recommendations collected from IEC TR 62095 [**?**] were used.

The heat conduction equation used [**? ? ? ? ? ?**], was as follows:

$$\frac{\partial}{\partial x}\left(k\frac{\partial \theta}{\partial x}\right)+\frac{\partial}{\partial y}\left(k\frac{\partial \theta}{\partial y}\right)=-q \tag{13}$$

where, θ is the temperature at any point in the x-y plane (K), k is the thermal conductivity $(W/m\cdot K)$ and q is the volumetric heat source (W/m^3).

As the simulations were performed in a steady state, it was unnecessary to perform iterations to adjust the losses with the temperature of the conductor as indicated in IEC TR 62095 [**?**]; it was sufficient to calculate the internal heat generation at the maximum admissible cable temperature of 90 $^\circ C$. In addition, to simplify the model, it was assumed that conductor losses, dielectric losses (practically zero) and sheath losses were all generated in aluminium. This assumption was validated by the experimental measurements.

The geometry created was a square with a height of 10 m and a width of 10 m. It was assumed that the left, right and bottom edges of the medium were perfectly insulated because they were widely separated from the heat generation by the cable. Convective heat transfer was considered for the upper edge, at an ambient temperature of 20 $^\circ C$ and a convective coefficient of 10 $W/m^2\cdot K$ corresponding to natural convection.

Figure 4 shows the generated mesh of the simulated model for a 0.5 m buried-depth cable and the location of the temperature probe.

Figure 4: Detail of mesh around underground cable and temperature probe.

The values of the thermal conductivities of the materials used in the models are shown in Table 2. The thermal conductivity of the soil used represents the value recommended for Spain according to [**? ?**], and the thermal conductivity of the sand was obtained from the simulations to calibrate the model. The remainder of the thermal conductivities were obtained from [**? ?**].

Table 2: Characteristics of materials used in simulations

Material	Thermal Conductivity $(W/m \cdot K)$	Specific Heat, C_P $(J/kg \cdot K)$	Density (kg/m^3)
Aluminium	237.5	951	2689
Polyethylene	0.4	2300	930
Sand	0.6667	920	1500
Soil	0.6667	1460	1800

3.3. Numerical model validation

To validate the created numerical model, the results obtained from the FEM model were compared with those obtained from the experimental measurements. The temperature trends obtained with the FEM model and the experimental measurements provided by the PT100 probes installed inside the sand and around the cable (Figs. 1 and 3) were compared and used to determine the most accurate value of the thermal conductivity of the sand.

Several experiments were performed to obtain the largest amount of comparison data. In these experiments, the current flowing through the conductor was the most important variable, and values from 126.5 to 367 A were obtained. In addition, one parameter that varied in the experimental tests was the ambient temperature, which was considered in the simulations of the FEM model.

Figure 5 shows the comparison of three experimental tests with different currents and their respective simulations in the FEM model; the x-axis represents the time in hours, and the temperature increment (ΔT) is represented on the y-axis. The temperature increment is given by

$$\Delta T = T_{probe_j} - T_{initial} \tag{14}$$

where, T_{probe_j} is the temperature measured by the probe in time, j is the number of probes and $T_{initial}$ is the initial temperature of the cable.

The series of simulations represented in Fig. 5 followed the same temperature trend as the series of experimental data. The maximum deviation ratio between the measured and simulated temperatures was 0.87%; therefore, the numerical model proposed can be considered valid and used to examine how the variation in cable installation depth influences cable temperature.

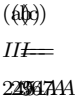

Figure 5: Comparison of data obtained from experimental measurements and numerical model using different currents: (a) $I = 245\ A$, (b) $I = 294\ A$ and (c) $I = 367\ A$.

4. Results

4.1. Ampacity calculation

For the ampacity calculation as a function of depth, Eqs. 1, 2, and 11 were used, which correspond to the different methods explained above; in addition, it was calculated for three different scenarios. These scenarios correspond to the values of thermal resistivity of wet, dry and very dry soil according to [**?**], with values of 1, 1.5, and 3 $K \cdot m/W$, respectively. Table 3 shows the values of thermal resistivity of soil used to calculate the ratio of the thermal resistivities of the dry and moist soil zones (υ), used in the Eq. 2 in each of the three scenarios discussed above. The critical temperature of the soil and temperature of the boundary between the dry and moist zones (θ_x), used in Eq. 2 was 60 $°C$ according to [**?** **?**]. The conductor temperature rise above the ambient temperature ($\Delta\theta$), used in Eqs. 1 and 2 was 70 $°C$, considering the maximum allowed temperature of the conductor at continuous load, 90 $°C$, according to the cable manufacturer and the ambient temperature, 20 $°C$, according to [**?**].

Table 3: Values of thermal resistivity of soil used in calculations

Scenario	Thermal resistivity		Ratio of the thermal resistivities, υ
	Moist soil, ρ_w $(K \cdot m/W)$	Dry soil, ρ_d $(K \cdot m/W)$	
1	0.75	1	1.33
2	1	1.5	1.5
3	1.5	3	2

Figure 6 shows the obtained permissible current rating of the buried cable in each scenario depending on cable depth. The shaded area between 0.6 and 1.5 m represents the typical cable depth in Spain according to IEC 60287-3-1 [**?**].

The ampacities calculated from IEC 60287-1-1 were kept parallel in the three cases and separated as the soil resistivity increased. The ampacity calculated from UNE 211435 as the soil resistivity increased was close to the ampacity of IEC 60287 where a partial drying-out of soil occurred and was closer to and even exceeded the ampacity of IEC 60287 where the drying-out of soil did not occur.

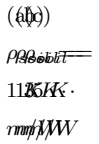

Figure 6: Ampacity calculated using different methods in three scenarios: (a) $\rho_{soil} = 1\ K \cdot m/W$, (b) $\rho_{soil} = 1.5\ K \cdot m/W$ and (c) $\rho_{soil} = 3\ K \cdot m/W$.

Table 4 shows the percentage of error ($I\%$) between the cable ampacities described above and the cable ampacity obtained in the simulations at each of the cable depths according to the following expression:

$$I(\%) = \frac{I_i - I_{simulated}}{I_{simulated}} \cdot 100 \tag{15}$$

where, I_i corresponds to each of the ampacities calculated from the standards and $I_{simulated}$ is the simulated ampacity.

Considering the typical cable depths in Spain [**?**], it was observed that the ampacity of IEC 60287 where partial drying-out of the soil occurred in the first two scenarios was the most accurate method of the two standards used in the range 1.49–2.33% and -0.33 to -0.80%, respectively. In the third scenario of very dry soil, it was observed that the calculated ampacity of IEC 60287 where partial drying-out of the soil occurred was more restrictive than the ampacity obtained through the simulated model in the range -10.49 to -10.11%.

The ampacities calculated from IEC 60287 where drying-out of the soil did not occur and UNE 211435 were above those obtained from the numerical model in all cases; therefore, the temperature of these ampacities will always be higher than the maximum permissible cable temperature. In the case of UNE 211435 when the depth was $\leq\ 0.6\ m$, the difference between ampacities was in the 1.64–2.3%, range; therefore, the temperature was very close to the simulated model temperature.

Table 4: Difference of ampacity with respect to simulated model ampacity

Cable Depth (m)	$\rho_{soil} = 1\ K \cdot m/W$			$\rho_{soil} = 1.5\ K \cdot m/W$			$\rho_{soil} = 3\ K \cdot m/W$		
	UNE 211435	**IEC 60287 (without drying-out)**	**IEC 60287 (with drying-out)**	**UNE 211435**	**IEC 60287 (without drying-out)**	**IEC 60287 (with drying-out)**	**UNE 211435**	**IEC 60287 (without drying-out)**	**IEC 60287 (with drying-out)**
0.5	2.30%	7.41%	2.84%	1.74%	5.94%	0.04%	1.85%	4.24%	-10.09%
0.6	1.98%	6.99%	2.33%	1.64%	5.64%	-0.33%	2.04%	4.09%	-10.31%
0.8	2.67%	6.59%	1.79%	2.63%	5.37%	-0.70%	3.43%	4.03%	-10.48%
1	2.79%	6.45%	1.56%	2.97%	5.35%	-0.80%	4.03%	4.13%	-10.49%
1.25	2.94%	6.48%	1.49%	3.33%	5.48%	-0.75%	4.63%	4.37%	-10.36%
1.5	3.80%	6.66%	1.60%	4.36%	5.76%	-0.55%	5.87%	4.73%	-10.11%
1.75	4.48%	6.99%	1.85%	5.13%	6.11%	-0.27%	6.82%	5.15%	-9.79%
2	4.96%	7.34%	2.14%	5.74%	6.53%	0.10%	7.55%	5.62%	-9.42%
2.5	5.62%	8.26%	2.94%	6.57%	7.53%	0.97%	8.61%	6.72%	-8.54%
3	7.13%	9.35%	3.91%	8.22%	8.67%	2.00%	10.49%	7.96%	-7.53%

4.2. Temperature calculation based on ampacity

From the ampacities calculated by the different methods, losses in the cable were obtained from Eqs. 8, 9 and 10. These losses were used in the simulated model to calculate the maximum temperature that occurs in a cable in steady state. Figure 7 shows the temperatures obtained based on the ampacity and cable depth.

As expected, the temperatures obtained from the calculated ampacities of UNE 211435 and IEC 60287 where drying-out of the soil did not occur are above 90 $^{\circ}C$ (Table 5). The temperatures of IEC 60287 where drying-out of the soil did not occur decreased the temperature difference with the simulated model as the soil resistivity increased. While the opposite occurred with the temperature obtained from UNE 211435, the temperature difference was greater as the soil resistivity increased. It is necessary to point out that both the ampacity (Fig. 6) and the temperature (Fig. 7) at depths $\leq$ 0.6 m of UNE 211435 adjusted best to the maximum permissible cable temperature, but as the depth increased in scenario 3 (very dry soil), the difference of temperature also increased, and it became the worst of the three methods.

The temperatures obtained (Table 5) by the calculated ampacities of IEC 60287 where partial drying-out of the soil occurred, behaved like the ampacity of Fig. 6. In the first two scenarios, the temperature was very close to the allowed 90 $^{\circ}C$ and the difference of temperature increased as the depth increased. In the third case, the temperature of the cable was less than the allowed maximum in the range 10.33–14.43 $^{\circ}C$ below because the calculated ampacity was more restrictive compared to that obtained by the simulated model.

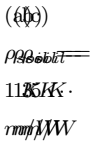

Figure 7: Results of temperatures obtained from simulated model based on ampacities: (a) $\rho_{soil} = 1\ K \cdot m/W$, (b) $\rho_{soil} = 1.5\ K \cdot m/W$ and (c) $\rho_{soil} = 3\ K \cdot m/W$.

Table 5: Difference of temperature with respect to maximum permissible cable temperature

Cable Depth (m)	$\rho_{soil} = 1\ K \cdot m/W$			$\rho_{soil} = 1.5\ K \cdot m/W$			$\rho_{soil} = 3\ K \cdot m/W$		
	UNE 211435 ($°C$)	**IEC 60287 (without drying-out)** ($°C$)	**IEC 60287 (with drying-out)** ($°C$)	**UNE 211435** ($°C$)	**IEC 60287 (without drying-out)** ($°C$)	**IEC 60287 (with drying-out)** ($°C$)	**UNE 211435** ($°C$)	**IEC 60287 (without drying-out)** ($°C$)	**IEC 60287 (with drying-out)** ($°C$)
0.5	0.489	7.717	1.238	0.370	6.307	-1.960	1.459	4.847	-14.293
0.6	0.505	7.604	0.991	0.581	6.240	-2.127	1.931	4.848	-14.398
0.8	2.003	7.590	0.771	2.377	6.297	-2.241	4.148	5.007	-14.430
1	2.496	7.741	0.765	3.090	6.506	-2.167	5.162	5.294	-14.323
1.25	2.981	8.079	0.940	3.791	6.904	-1.917	6.157	5.771	-14.067
1.5	4.385	8.538	1.255	5.383	7.416	-1.542	8.023	6.349	-13.712
1.75	5.433	9.092	1.677	6.593	8.018	-1.071	9.466	7.012	-13.282
2	6.226	9.726	2.184	7.529	8.698	-0.522	10.605	7.749	-12.788
2.5	7.276	11.192	3.404	8.824	10.252	0.767	12.243	9.409	-11.644
3	9.543	12.871	4.839	11.335	12.015	2.258	15.117	11.274	-10.333

4.3. Effect of cable depth based on ampacity

To observe the influence of the cable depth on its temperature, the ampacities calculated for a 1 m depth and a soil resistivity of 1.5 $K \cdot m/W$ of the three methods and the simulated model shown in Fig. 6b (Zone A) were used. Figure 8 shows the temperature variation for both the standards and the simulation as a function of cable depth with cable currents of 276.7, 270.4, 262.6 and 260.5 A. For the same current, a difference of 29.98–32.30 $°C$ was obtained between the lowest and highest cable depth.

Figure 8: Temperature variation depending on cable depth and current.

5. Conclusions

This article presented a thermal analysis of medium-voltage underground cables. A small-scale model of a buried cable was constructed to validate the generated simulated model. The cables were in a trefoil

formation. The cable depths varied from 0.5 to 3 m. The variation of ampacity was studied as a function of soil resistivity (wet, dry and very dry soil) and cable depth. The ampacities were calculated by three methods of existing standards and through the created simulated model. In addition, FEM thermal analysis was performed to determine the maximum steady-state temperature obtained from the calculated ampacities. Finally, the magnetic field generated as a function of cable installation depth and the calculated ampacities was studied. The analyses results of the medium-voltage underground cable are summarized as follows.

- The maximum temperature of the cable increases with an increase in installation depth.
- Standard IEC 60287 indicates that the most restrictive ampacity obtained from their methodologies is used. The calculated ampacities where soil drying-out does not occur are always above those of the simulated model, which transforms into a temperature above the maximum permissible cable temperature.
- The calculation of ampacity using the UNE 211435 standard is almost always between that of the two IEC 60287 methods. However, when the cable depth is increased, it moves away from the ideal ampacity obtained from the simulated model. At depths $\leq 0.6\ m$, the use of this method for ampacity calculation is adequate.
- According to Table 4, the ampacity of the IEC 60287 standard where partial drying-out of the soil occurs is in the range 0.04–3.91% above and 0.27–0.8% below that of the simulated model ampacity in wet and dry soil conditions; these ranges can be considered as adequate. In very dry soil conditions, the ampacity range is 7.53–10.49% below that of the simulated model ampacity, which transforms into 12.55–21.03 A less than the simulated model.

To perform the dynamic management of a distribution network, it is necessary to study the behaviour of cables in steady-state with knowledge of the thermal resistivities of all elements that influence the final temperature of the cable and the application of the standards [**?**][**?**].

Acknowledgements

This work was supported by the Spanish government under the Spanish R+D initiative with references ENE-2013-42720-R and RETOS RTC-2015-3795-3, by the Cantabria government under the R+D initiatives with references SODERCAN/FEDER Proyectos Puente 2017 and by the University of Cantabria Industrial Doctorate 19.DI12.649. The authors also acknowledge support from Viesgo.

References

[1] CIGRE Technical Brochure 338, Statistics Of AC Underground Cables In Power Networks (dec 1998).

[2] IEEE Std 399-1997, IEEE Recommended Practice for Industrial and Commercial Power Systems Analysis (Brown Book) (1998). doi:10.1109/IEEESTD.1998.88568.

[3] IEC 60853-1:1985 Calculation of the cyclic and emergency current rating of cables. Cyclic rating factor for cables up to and including 18/30 (36) kV (1985).

[4] IEC 60853-2:1989 Calculation of the cyclic and emergency current rating of cables. Cyclic rating of cables greater than 18/30 (36) kV and emergency ratings for cables of all voltages (1989).

[5] M. Rasoulpoor, M. Mirzaie, S. Mirimani, Thermal assessment of sheathed medium voltage power cables under non-sinusoidal current and daily load cycle, Applied Thermal Engineering 123 (2017) 353–364. doi:10.1016/j.applthermaleng.2017.05.070.

[6] M. Diaz-Aguilo, F. D. Leon, S. Jazebi, M. Terracciano, Ladder-type soil model for dynamic thermal rating of underground power cables, IEEE Power and Energy Technology Systems Journal 1 (2014) 21–30. doi:10.1109/jpets.2014.2365017.

[7] P. Chatzipanagiotou, V. Chatziathanasiou, G. D. Mey, B. Więcek, Influence of soil humidity on the thermal impedance, time constant and structure function of underground cables: A laboratory experiment, Applied Thermal Engineering 113 (2017) 1444–1451. doi:10.1016/j.applthermaleng.2016.11.117.

[8] I. Papagiannopoulos, V. Chatziathanasiou, L. Exizidis, G. Andreou, G. D. Mey, B. Więcek, Behaviour of the thermal impedance of buried power cables, International Journal of Electrical Power & Energy Systems 44 (1) (2013) 383–387. doi:10.1016/j.ijepes.2012.07.064.

[9] A. Sturchio, G. Fioriti, V. Salusest, L. Calcara, M. Pompili, Thermal behavior of distribution MV underground cables, in: 2015 AEIT International Annual Conference (AEIT), IEEE, 2015. doi:10.1109/aeit.2015.7415247.

[10] L. Calcara, S. Sangiovanni, M. Pompili, MV underground cables: Effects of soil thermal resistivity on anomalous working temperatures, in: 2017 AEIT International Annual Conference, IEEE, 2017. doi:10.23919/aeit.2017.8240508.

[11] F. Salata, F. Nardecchia, A. de Lieto Vollaro, F. Gugliermetti, Underground electric cables a correct evaluation of the soil thermal resistance, Applied Thermal Engineering 78 (2015) 268–277. doi:10.1016/j.applthermaleng.2014.12.059.

[12] F. Salata, V. de, V. de, A model for the evaluation of heat loss from underground cables in non-uniform soil to optimize the system design, Thermal Science 19 (2) (2015) 461–474. doi:10.2298/tsci120528119s.

[13] F. Salata, F. Nardecchia, F. Gugliermetti, A. de Lieto Vollaro, How thermal conductivity of excavation materials affects the behavior of underground power cables, Applied Thermal Engineering 100 (2016) 528–537. doi:10.1016/j.applthermaleng.2016.01.168.

[14] J. H. Shazly, M. A. Mostafa, D. K. Ibrahim, E. E. A. E. Zahab, Thermal analysis of high-voltage cables with several types of insulation for different configurations in the presence of harmonics, IET Generation, Transmission & Distribution 11 (14) (2017) 3439–3448. doi:10.1049/iet-gtd.2016.0862.

[15] C. Holyk, H.-D. Liess, S. Grondel, H. Kanbach, F. Loos, Simulation and measurement of the steady-state temperature in multi-core cables, Electric Power Systems Research 116 (2014) 54–66. doi:10.1016/j.epsr.2014.05.001.

[16] P. Vaucheret, R. Hartlein, W. Black, Ampacity derating factors for cables buried in short segments of conduit, IEEE Transactions on Power Delivery 20 (2) (2005) 560–565. doi:10.1109/tpwrd.2005.844358.

[17] M. Rasoulpoor, M. Mirzaie, S. M. Mirimani, Effects of non-sinusoidal current on current division, ampacity and magnetic field of parallel power cables, IET Science, Measurement & Technology 11 (5) (2017) 553–562. doi:10.1049/iet-smt.2016.0549.

[18] P. Ocłoń, P. Cisek, D. Taler, M. Pilarczyk, T. Szwarc, Optimizing of the underground power cable bedding using momentum-type particle swarm optimization method, Energy 92 (2015) 230–239. doi:10.1016/j.energy.2015.04.100.

[19] P. Ocłoń, P. Cisek, M. Pilarczyk, D. Taler, Numerical simulation of heat dissipation processes in underground power cable system situated in thermal backfill and buried in a multilayered soil, Energy Conversion and Management 95 (2015) 352–370. doi:10.1016/j.enconman.2015.01.092.

[20] M. Rerak, P. Ocłoń, Thermal analysis of underground power cable system, Journal of Thermal Science 26 (5) (2017) 465–471. doi:10.1007/s11630-017-0963-2.

[21] IEC 60287-1-1:2006 Electric cables – Calculation of the current rating – Part 1-1: Current rating equations (100% load factor) and calculation of losses – General (2006).

[22] AENOR, UNE 211435:2007, Guía para la elección de cables eléctricos de tensión asignada superior o igual a 0,6/1 kV para circuitos de distribución de energía eléctrica (2007).

[23] IEC 60287-2-1:2015 Electric cables – Calculation of the current rating – Part 2: Thermal resistance – Section 2.1: Calculation of thermal resistance (2015).

[24] S. Bustamante, P. Castro, A. Laso, M. Manana, A. Arroyo, Smart thermostats: An experimental facility to test their capabilities and savings potential, Sustainability 9 (8) (2017) 1462. doi:10.3390/su9081462.

[25] ANSYS®, Academic Research Mechanical, Release 19.0.

[26] IEC TR 62095:2003 Electric cables – Calculations for current ratings – Finite Element method (2003).

[27] O. E. Gouda, A. Z. E. Dein, G. M. Amer, Effect of the formation of the dry zone around underground power cables on their ratings, IEEE Transactions on Power Delivery 26 (2) (2011) 972–978. doi:10.1109/tpwrd.2010.2060369.

[28] IEC 60287-3-1:2017 Electric cables – Calculation of the current rating – Part 3-1: Operating conditions – Site reference conditions (2017).

[29] CIGRE Technical Brochure 640, A Guide for Rating Calculations of Insulated Cables (dec 1998).

[30] O. E. Gouda, G. M. Amer, A. Z. E. Dein, Effect of dry zone formation around underground power cables on their ratings, in: CIRED 2009 - 20th International Conference and Exhibition on Electricity Distribution - Part 1, 2009, pp. 1–6.

The highlights of this paper are:

- Numerical, experimental and simulated model of MV underground cables is presented
- A comparison of the IEC standard and UNE standard (simplified IEC) is performed
- The simplified standard is less accurate than the IEC (with dry zone formation)
- UNE 211435 has a minor error when depth is less than or equal to 0.6 m